

Monolithic AlN MEMS-CMOS Resonant Transformer for Wake-up Receivers

Jeronimo Segovia-Fernandez
Department of Mechanical and
Aerospace Engineering
University of California, Davis
Davis, CA, USA
jeronimo.segovia@gmail.com

Julius M. Tsai
InvenSense Inc.
San Jose, CA, USA
jtsai@invensense.com

James Do
Department of Electrical and
Computer Engineering
University of California, Davis
Davis, CA, USA
jtsdo@ucdavis.edu

Hooman Rashtian
Department of Electrical and
Computer Engineering
University of California, Davis
Davis, CA, USA
hrashtian@ucdavis.edu

Xiaonan Jiang
Department of Electrical and
Computer Engineering
University of California, Davis
Davis, CA, USA
xnjiang@ucdavis.edu

Xiaoguang Liu
Department of Electrical and
Computer Engineering
University of California, Davis
Davis, CA, USA
lxgliu@ucdavis.edu

Yuhao Liu
Department of Electrical and
Computer Engineering
University of California, Davis
Davis, CA, USA
yuhliu@ucdavis.edu

David A. Horsley
Department of Mechanical and
Aerospace Engineering
University of California, Davis
Davis, CA, USA
dahorsley@ucdavis.edu

Abstract—A monolithic piezoelectric MEMS-CMOS resonant transformer that can be used in ultra-low-power high-efficiency RF sensing applications is presented for the first time. The MEMS-CMOS resonant transformer is based on a 59 MHz 2-port Aluminum Nitride (AlN) Contour Mode Resonator (CMR) bonded to a 0.18 μm NMOS-based rectifier for voltage boosting and RF-to-DC conversion. The integrated device is fabricated in a foundry-based process by conductive eutectic wafer bonding. To amplify the voltage, the AlN CMR is designed to attain a large quality factor ($Q=900$) and a relatively low dielectric capacitance ($C_0=1.51$ pF) in relation to the number of rectifier stages ($n=20$). As a result, a ten-fold voltage gain MEMS-CMOS resonant transformer is demonstrated in this work.

Keywords—Piezoelectric resonant transformer, MEMS-CMOS, AlN Contour Mode Resonator, voltage boost, wake-up receiver.

I. INTRODUCTION

The concept of ubiquitous wireless sensor networks (WSN) that provide persistent and high spatial/temporal resolution sensing can be applied to a wide variety of Internet of Things (IoT) applications [1]. Although technology has progressed in developing miniature sensors and high efficiency microprocessors, the realization of unattended WSN with extended lifetime still remains a challenge. To overcome the battery constraint, RF receivers that stay dormant and can be woken-up by extremely faint signals have been proposed. The same approach has been followed to enable high-efficiency rectifiers that can convert the attenuated RF signal at the antenna into a readable DC output. However, state-of-the-art wake-up receivers employ either magnetic-core transformers that can be integrated but exhibit low Q at resonance (around 15) [2], [3] or surface acoustic wave (SAW) filters that exhibit large Q s but cannot be integrated with semiconductor-based technologies [4].

The adoption of piezoelectric MEMS resonators to replace low- Q magnetic transformers and bulky SAW filters in wake-up receivers offers an integrated solution to achieve network impedance matching and, at the same time, a large voltage boost between the antenna and output port [5]. Among all the

piezoelectric materials, AlN has become very popular in resonator applications due to its high electrical resistivity, homogenous nucleation of grains along the c -axis, and constant piezoelectric performance across the frequency of operation [6]. In relation to the resonator mode of vibration, Contour Mode Resonators (CMRs) have emerged as a new class of piezoelectric MEMS transducers that can offer on-chip frequency reconfiguration for future wireless communication systems. In comparison to film bulk acoustic resonators (FBARs) and shear-mode resonators, CMRs present an in-plane mode of vibration that is primarily defined by the resonator lateral dimensions and can be set lithographically [7], [8].

In this work, a monolithic piezoelectric MEMS-CMOS resonant transformer based on a 59 MHz 2-port AlN CMR with $Q = 900$ is presented. The integrated device was manufactured in a foundry-based process by conductive eutectic wafer bonding of a CMOS wafer containing a 0.18 μm NMOS-based rectifier to a MEMS wafer containing the 2-port AlN CMR. When operated slightly above the natural resonance frequency (f_r), the AlN CMR behaves as a high- Q inductor that can significantly boost the voltage swing at the rectifier input. The experimental outcome shows a ten-fold voltage boost in the rectification stage, resulting in an order of magnitude improvement in sensitivity/efficiency.

II. ALN CMR

The principle of operation of AlN CMRs has been described in literature [8]. The device is based on a piezoelectric plate sandwiched between two patterned metal layers that are employed to create an electric field across the thickness of the piezoelectric film (h). The top metal is formed by an array of interdigitated (IDT) electrodes that are alternatively connected to input (V_{in}) and output (V_{out}) ports while the bottom metal works as a common ground plate (Fig. 1.a). The electric field applied in the thickness direction generates a width-extensional mode of vibration in the AlN plate through the intrinsic d_{31} piezoelectric coefficient (Fig. 1.b). In this configuration, the electrode-pitch or finger width (W_f)

sets the acoustic wavelength (λ) of the excited mode (λ is equal to $2W_f$), so the resonance frequency (f_r) can be derived as:

$$f_r = \frac{1}{2W_f} \sqrt{\frac{E_{eq}}{\rho_{eq}}} \quad (1)$$

where E_{eq} and ρ_{eq} represent respectively the equivalent Young's modulus and mass density of the multilayer stack forming the device. For this work, a resonator with $f_r=59$ MHz corresponding to $W_f=80 \mu\text{m}$ is fabricated and tested.

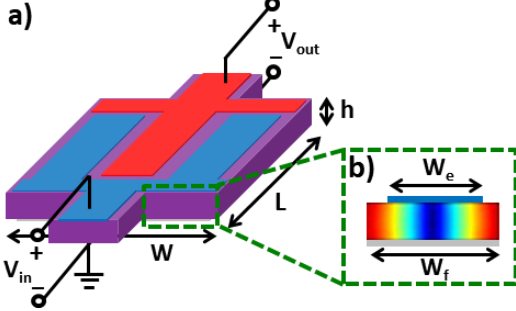


Fig. 1. a) 3D view of a 2-port AlN CMR and b) cross section representation of one finger exhibiting a width-extensional mode of vibration.

The 2-port AlN CMR can be modeled as a one-degree-of-freedom system in the electrical domain. The equivalent stiffness, damping, and mass of each resonator finger are respectively represented by the motional capacitance (C_M), resistance (R_M), and inductance (L_M). This circuit is known as the modified Butterworth Van-Dyke (mBVD) model as it also includes the parasitic capacitance that accounts for the dielectric polarization of the piezoelectric layer (C_0). Fig. 2 shows the electrical representation of the 2-port AlN CMR employed in this work, which has 2 input fingers connected in parallel to V_{in} and 1 output finger solely connected to V_{out} .

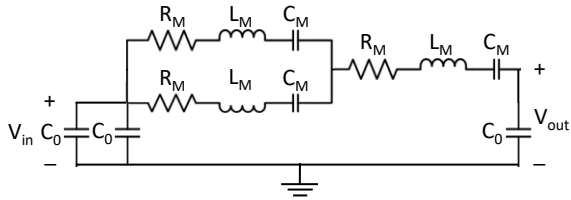


Fig. 2. Equivalent modified Butterworth Van-Dyke (mBVD) model of a 2-port AlN CMR having 2 input fingers and 1 output finger.

For practical applications, such as the use of these 2-port AlN CMRs to build RF resonant transformers, it is convenient to express the equivalent motional parameters (R_M , L_M , and C_M) in terms of the dielectric capacitance (C_0), Q , k_t^2 , and the angular resonance frequency ($\omega_r=2\pi f_r$) of the resonator. In the linear regime, the motional parameters can be obtained as follows:

$$R_M = \frac{\pi^2}{8} \frac{1}{C_0 \omega_r k_t^2 Q}; C_M = \frac{8}{\pi^2} k_t^2 C_0; L_M = \frac{\pi^2}{8} \frac{1}{\omega_r^2 k_t^2 C_0} \quad (2)$$

The electromechanical coupling (k_t^2) is a measure of the resonator efficiency and can be defined as the ratio of mechanical energy and supplied electrical energy. In the case

of a one finger resonator with a partially-electroded piezoelectric plate surface, such as it is shown in Fig. 1.b, the amplitude of vibration at f_r depends on W_e . According to [9], the effective k_t^2 of such resonator topology assuming 1D mode of vibration becomes proportional to the following factor:

$$k_t^2 \propto \frac{W_f}{W_e} \left[\sin\left(\frac{\pi W_e}{2 W_f}\right) \right]^2 \quad (3)$$

where W_e/W_f represents the electrode-to-finger width ratio. This formula translates into a maximum k_t^2 when $W_e/W_f=0.75$, which is the value selected to design the AlN CMR for this work. The absolute k_t^2 can be computed via FEM techniques by applying the following equation that relates k_t^2 to the f_r and parallel frequency (f_p) of the simulated admittance:

$$k_t^2 = \frac{\pi^2}{8} \frac{f_p^2 - f_r^2}{f_r^2} \quad (4)$$

The Q is a measure of the sharpness of the resonator response and it is defined as the ratio between the energy stored and the rate of energy lost per cycle of vibration in the device. Previous studies [10] on this class of MEMS resonators have demonstrated that Q is dominated by anchor losses in the very high frequency (VHF) range (this coincides with the frequency range of application). To model anchor losses, which are due to the scattering of elastic waves from the resonator into the substrate through the anchors, FEM involving the use of Fixed Constraint (FC) boundary conditions are implemented [11]. Based on FC-FEM simulations, the resonator length (L) is set to $344 \mu\text{m}$ in order to maximize Q due to anchor losses.

III. NMOS RECTIFIER

NMOS rectifiers are usually constructed by using diode-connected NMOS transistors (Fig. 3). The input impedance of the circuit is capacitive and equivalent to $Z_{in} = R_n - jX_n$, in which $R_n = R_1/n$, $X_n = nX_1$, and R_1 and X_1 represent the resistance and reactance of each of the stages in an n-stage rectifier, respectively. A limiting factor in the performance of NMOS rectifiers is the large impedance mismatch that exists between their input and antenna ports (R_{ant}). If the rectifier is modeled by a parallel RC circuit, the parallel resistance is given by $R_p = (R_n^2 + X_n^2)/R_n$, which is significantly larger than 50Ω . To maximize the energy transference and increase the minimum detectable RF signal, the 2-port AlN CMR operating in the inductive region ($f > f_r$) is introduced between the antenna and rectifier stage.

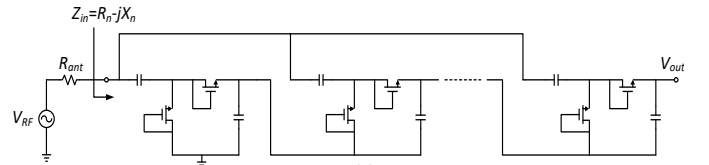


Fig. 3: N-stage MOS rectifier connected to the RF antenna.

If we model the 2-port AlN CMR as a single inductor resonating with the capacitive part of the rectifier input impedance (Fig. 4.a), the magnitude of the current phasor in the

loop is maximized and the voltage at the input of the rectifier is boosted. The equation for the voltage phasor at the input of the rectifier can be written as:

$$V_{in} = \frac{\sqrt{X_n^2 + R_n^2}}{R_n + R_{ant}} V_{RF} \approx \frac{X_n}{R_n + R_{ant}} V_{RF} \quad (5)$$

From (5), the higher the value of reactance at the input impedance of the rectifier (X_n) compared with $R_n + R_{ant}$, the higher the voltage boosting that can be obtained. While this approach can improve the sensitivity of the CMOS rectifier, its effectiveness is strongly dependent on the C_0 , Q , k_t^2 of the piezoelectric resonator employed. By substituting the matching inductor by a more realistic model of the 2-port AIN CMR (Fig. 4.b), the equation for the voltage boost (or gain) needs to be rewritten as follows:

$$\frac{V_{in}}{V_{RF}} \approx \frac{1}{j\omega(C_0 + C_n)(R_{ant} + R'_m)} V_{RF} \quad (6)$$

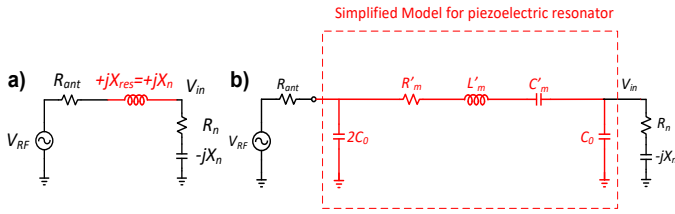


Fig. 4. Incorporation of a) a series inductor and b) a series RLC circuit equivalent to a 2-port AIN CMR as a voltage boosting network to increase the level of signal applied to the MOS rectifier.

As mentioned before, the voltage conversion gain of the rectifier can be increased linearly by increasing the number of stages (n) [12]:

$$V_{out,DC} = \frac{nV_{in}^2}{2V_T} \quad (7)$$

However, this comes at the price of increasing the input capacitance of the rectifier (C_n) as the additional stages can be considered to be in parallel. Eq. (6) indicates that increasing the value C_n results in lowering the voltage boost that can be obtained. By replacing (7) into (6), we get the following equation for $V_{out,DC}$:

$$V_{out,DC} = \frac{nV_{RF}^2}{2\omega^2(R_{ant} + R'_m)^2(C_0 + nC_1)^2} \quad (8)$$

The size of the NMOS transistor used in this work is 5 μm that corresponds to $C_j = 345$ fF. n was set to be 20 for this preliminary transformer design, which results into a voltage boost that is approximately 10 times.

IV. MEMS-CMOS PROCESS

The AIN MEMS-CMOS fabrication process used to build the piezoelectric resonant transformer described in this paper employs two starting wafers (MEMS and CMOS) [13]. The MEMS wafer (Fig. 5.a) is first patterned with back-side alignment marks used for front-to-back alignment after fusion bonding. The MEMS wafer is then deposited with AIN seed,

Mo bottom electrode (150 nm), AIN piezoelectric (1 μm) and SiO_2 standoff layers, where both Mo and SiO_2 standoff layers are patterned. The standoff layer is formed on the MEMS wafer to provide separation between the MEMS structure and the CMOS wafer. Later, the AIN piezoelectric layer is etched twice; first to define the resonator geometry and second to form the Mo bottom electrode contact by open VIAS. Al, Ti and Ge are then deposited in sequence from bottom to top and patterned in order to define the Al top electrode (150 nm) and Ge bonding pads.

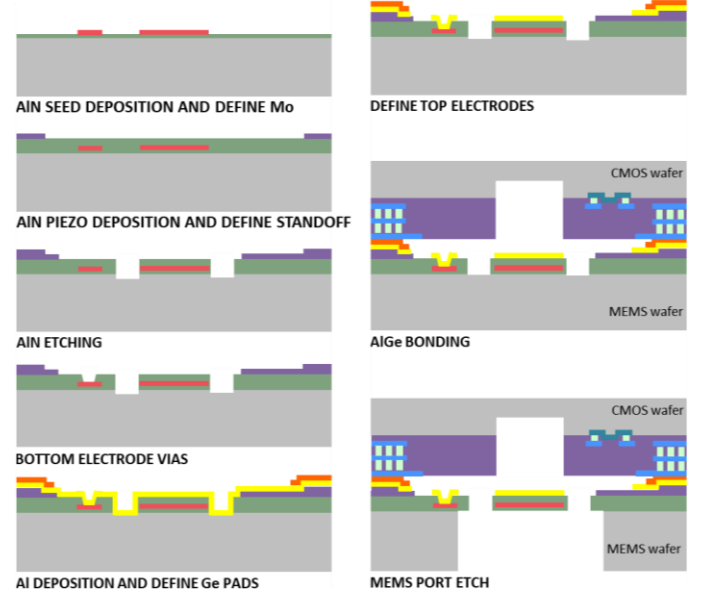


Fig. 5: Piezoelectric transformer fabrication steps including a) MEMS wafer and b) MEMS-CMOS integration process flows.

A bottom cavity is etched in the CMOS wafer (Fig. 5.b) to allow clearance for the moving AIN CMR. The MEMS and CMOS wafers are then bonded using an Al-Ge eutectic bond to create a hermetic seal around the MEMS structures as well as electrical interconnects between the MEMS resonator and CMOS circuit. Finally, after thinning the MEMS wafer to 200 μm thickness by grinding, the MEMS port is etched through the MEMS wafer to completely release the MEMS resonator from the Si substrate.

V. EXPERIMENTAL DATA ANALYSIS

To extract the electrical parameters of the integrated AIN MEMS-CMOS resonant transformer an Agilent E5071A 300kHz-8.5GHz Network Analyzer is utilized. The measured S_{11} -parameter at the antenna port (the output port was left open) is converted into Y_{11} -parameter (or admittance) and fitted to the simplified model of the piezoelectric resonant transformer (see Fig. 4.b). For the specific circuit under test, $R_m = 112.08 \Omega$, $L_m = 0.27$ mH, $C_m = 27.98$ fF, and $C_0 = 1.51$ pF assuming that $C_j = 345$ fF. The fitted magnitude and phase of the measured admittance are plotted in Fig. 6.

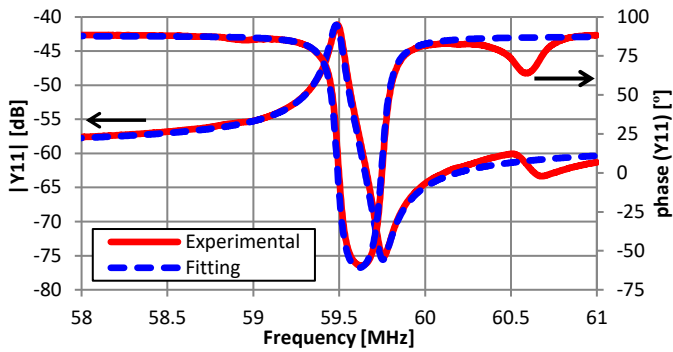


Fig. 6. Fitted admittance response of the AlN MEMS-CMOS resonant transformer.

To determine the voltage gain of the RF-DC AlN MEMS-CMOS transformer we connected the DC output port to a RIGOL DS1102E oscilloscope which has an input impedance greater than $1\text{ M}\Omega$ to avoid loading the rectifier output. Then, the input RF signal was swept from 59.35 to 59.6 MHz around resonance to capture the maximum voltage amplification. Fig. 7 plots the voltage gain of the receiver calculated as the ratio of output DC voltage and input RF voltage in rms value. Here the data points correspond to the experimental values and the solid line corresponds to the predicted values assuming the equivalent circuit parameters previously fitted. As we can see, both plots show very good correlation.

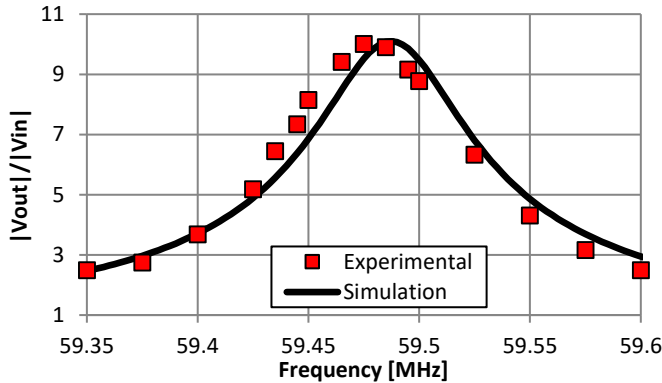


Fig. 7. Experimental and simulated voltage gain of the AlN MEMS-CMOS resonant transformer.

VI. CONCLUSIONS

A monolithic piezoelectric MEMS-CMOS resonant transformer based on a 59 MHz 2-port AlN CMR with $Q=900$ bonded to a $0.18\text{ }\mu\text{m}$ NMOS-based rectifier has been presented in this paper. The AlN CMR consists of a $1\text{ }\mu\text{m}$ -thick AlN slab sandwiched between a 150 nm -thick Mo ground plate and a 150 nm -thick Al IDT top electrode whose pitch is $80\text{ }\mu\text{m}$. The

electrode coverage and resonator length have been designed to be 0.75 and $344\text{ }\mu\text{m}$ in order to maximize k_t^2 and Q according to FEM simulations. To maximize the energy transference and boost the RF-to-DC voltage, the AlN CMR operates in the inductive region ($f > f_r$) and the number of rectifier stages is optimized ($n=20$) based on the AlN CMR dielectric capacitance ($C_0=1.51\text{ pF}$). The integrated device, which was fabricated by eutectic bonding of MEMS and CMOS wafers, provides with a ten-fold voltage boost in the rectification stage, resulting in an order of magnitude improvement in sensitivity/efficiency.

ACKNOWLEDGMENT

This work was sponsored by DARPA, Microsystems Technology Office under the N-ZERO Program, Contract HR0011-15-C-0145.

REFERENCES

- [1] N. Khalil, M. R. Abid, D. Benhaddou, and M. Gerndt, "Wireless sensors networks for Internet of Things," in *2014 IEEE Ninth International Conference on Intelligent Sensors, Sensor Networks and Information Processing (ISSNIP)*, 2014, pp. 1–6.
- [2] N. M. Pletcher, S. Gambini, and J. Rabaey, "A $52\text{ }\mu\text{W}$ Wake-Up Receiver With -72 dBm Sensitivity Using an Uncertain-IF Architecture," *IEEE J. Solid-State Circuits*, vol. 44, no. 1, pp. 269–280, Jan. 2009.
- [3] J. Bae and H. J. Yoo, "A $45\text{ }\mu\text{W}$ Injection-Locked FSK Wake-Up Receiver With Frequency-to-Envelope Conversion for Crystal-Less Wireless Body Area Network," *IEEE J. Solid-State Circuits*, vol. 50, no. 6, pp. 1351–1360, Jun. 2015.
- [4] S. Moazzeni, M. Sawan, and G. E. R. Cowan, "An Ultra-Low-Power Energy-Efficient Dual-Mode Wake-Up Receiver," *IEEE Trans. Circuits Syst. Regul. Pap.*, vol. 62, no. 2, pp. 517–526, Feb. 2015.
- [5] R. H. Olsson, K. E. Wojciechowski, M. R. Tuck, and J. E. Stevens, "Microresonant impedance transformers," in *2009 IEEE International Ultrasonics Symposium*, 2009, pp. 2153–2157.
- [6] S. Trolhier-McKinstry and P. Muralt, "Thin Film Piezoelectrics for MEMS," *J. Electroceramics*, vol. 12, no. 1–2, pp. 7–17, Jan. 2004.
- [7] G. Piazza, P. J. Stephanou, and A. P. Pisano, "Piezoelectric Aluminum Nitride Vibrating Contour-Mode MEMS Resonators," *J. Microelectromechanical Syst.*, vol. 15, no. 6, pp. 1406–1418, Dec. 2006.
- [8] M. Rinaldi, C. Zuniga, C. Zuo, and G. Piazza, "Super-high-frequency two-port AlN contour-mode resonators for RF applications," *IEEE Trans. Ultrason. Ferroelectr. Freq. Control*, vol. 57, no. 1, pp. 38–45, Jan. 2010.
- [9] W. G. Cady, *Piezoelectricity: An Introduction to the Theory and Applications of Electromechanical Phenomena In Crystals*, 1st edition. McGraw-Hill, 1946.
- [10] J. Segovia-Fernandez, M. Cremonesi, C. Cassella, A. Frangi, and G. Piazza, "Anchor Losses in AlN Contour Mode Resonators," *J. Microelectromechanical Syst.*, vol. 24, no. 2, pp. 265–275, Apr. 2015.
- [11] J. Segovia-Fernandez and G. Piazza, "Analytical and Numerical Methods to Model Anchor Losses in 65-MHz AlN Contour Mode Resonators," *J. Microelectromechanical Syst.*, vol. 25, no. 3, pp. 459–468, Jun. 2016.
- [12] S. T. Block *et al.*, "A 100-nW CMOS Wake-up Receiver with -60 dBm Sensitivity Using AlN High-Q Piezoelectric Resonators," presented at the IEEE International Symposium on Circuits and Systems (ISCAS), 2017.
- [13] J. M. Tsai *et al.*, "Versatile CMOS-MEMS integrated piezoelectric platform," in *2015 Transducers - 2015 18th International Conference on Solid-State Sensors, Actuators and Microsystems (TRANSDUCERS)*, 2015, pp. 2248–2251.